

Recovering the structure of a layered soil, including layer thickness and dielectric permittivity, using the interfaces and objects backscatter detected in GPR B-scans

M.R. Ardekani*, P. Druyts*, S. Lambot[†], A. De Coster[†], X. Neyt*

*Signal and Image Centre, Royal Military Academy, 30 Avenue de la Renaissance, 1000 Brussels, Belgium

[†]Earth and Life Institute, Université catholique de Louvain, Croix du Sud 2 Box L7.05.02, 1348 LLN, Belgium
Mohammad.Mahmoudzadeh@elec.rma.ac.be

Abstract—It is well-known that point scatterers appear as hyperbolas in ground-penetrating radar (GPR) B-scans and that the layer interfaces appear as horizontal lines. In this paper the shape and location of the hyperbolas, together with the location of the layer interfaces, are used to estimate the soil dielectric permittivity for a layered soil. For this, a procedure composed of following steps is used: (1) reflection detection, (2) hyperbola detection, (3) refinement of hyperbola parameters and estimation of the corresponding scatterer location and soil effective dielectric permittivity, and (4) computation of scatterer depth and layer permittivity taking into account the properties of the upper layers. The reflection detection step takes the GPR B-scan as input and produces a ‘reflection binary image’ as output. The binary image highlights reflections of interest, which includes the hyperbolas and the soil layer interfaces. The effective soil dielectric permittivity is estimated by fitting a theoretically computed hyperbola to the ‘reflection binary image’ for each reflection detected. Then, hyperbola parameters are refined by optimizing a cost function which is computed on the original B-scan for each detected hyperbola. Finally, the soil layer dielectric permittivity and scatterer depth are derived from the hyperbola parameters, taking into account the properties of the upper layers. The procedure is applied to simulated data, showing good accuracy in soil dielectric permittivity estimation and high computational efficiency.

Index Terms—Ground-penetrating radar, hyperbola detection, soil dielectric permittivity retrieval.

I. INTRODUCTION

Ground-penetrating radar (GPR) is one of the geophysical tools which is used for soil dielectric permittivity estimation and buried object detection. The soil dielectric permittivity influences the electromagnetic wave propagation velocity which can be estimated from the measured echo signal. Also, if the soil contains distinguishable layers, the dielectric permittivities of the adjacent layers influence the electromagnetic reflection coefficient of the corresponding subsurface, which can be used for the estimation of soil dielectric permittivity. There are several approaches for layered soil dielectric permittivity estimation, namely, common mid-point (CMP) [1], wide angle reflection and refraction (WARR) [2], and full-wave inversion [3]–[5]. The CMP and WARR require several measurements

for the characterization of a single profile and GPR full-wave inversion requires accurate GPR calibration for layered soil reconstruction [6].

GPR is also used to detect buried objects [7]. It is well-known that point scatterer appears as a hyperbola in GPR B-scan. To detect the hyperbolas, the Hough transform has been widely used, which also provides an estimation of effective soil dielectric permittivity [8]. Migration of GPR data is also a method to estimate the effective soil dielectric permittivity and detect the buried objects [9]. Approaches based on the Hough transform and migration based methods are computational intensive.

The method presented in this paper aims at characterizing the layered soil structure, including and estimation of the number of layers together with their permittivities and thicknesses. This is done by detection isolated objects and by fitting a parameterized response. The permittivity of each layer is then recursively obtained starting from the top-most layer. One of the key aspect of the method is its computational efficiency.

II. PROCESSING PROCEDURE

The proposed procedure is composed of four processing steps, namely, detection of reflections, the hyperbola detection to determine if the detected reflections actually correspond to a point scatterer and to provide an initial estimate of the effective soil permittivity and scatterer location, refinement of the hyperbola parameters, and extraction of scatterer depth and layer permittivity taking into account the properties of the upper layers.

A. Reflection detection

The reflection detection is a modified version of the method presented in [10]. In summary, reflections appearing in each 1D GPR signal (A-scans) are detected using the knowledge that such a reflection appears as a delayed version of the transmitted signal, i.e. a ricker pulse for the GPR considered in this paper. Applying such a procedure to all the A-scans composing a B-scan, a binary image is created from the detected reflections. In order to bridge the small gaps between the

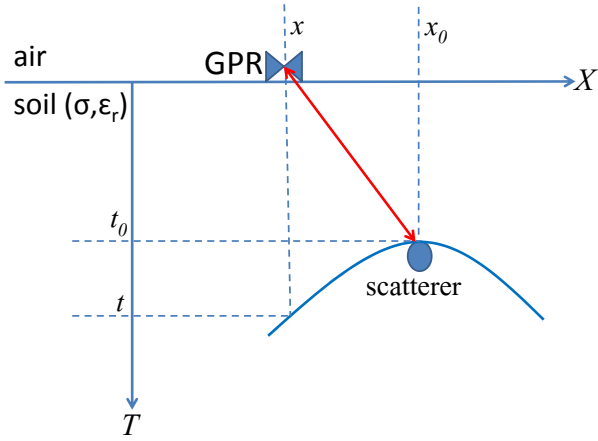


Fig. 1: Reflections due to an object in (x_0, t_0) . 'GPR' represents the location of the transmitter and receiver antennas.

detections, a dilation operation with a rectangular structuring element is applied to the binary image. The time-domain size of the structuring element is chosen equal to half the duration of the pulse transmitted by the GPR and the GPR position domain dimension size of the structuring element corresponds to 2 pixels. In addition, the reflections from the soil interfaces between layers are detected and will be used for soil layer thickness estimation.

B. Hyperbola detection

The next step includes the hyperbola detection and the estimation of the related parameters which are linked to the soil effective dielectric permittivity and scatterer location. For a homogeneous full-space, the reflections corresponding to a scatterer (an object) located in (x_0, t_0) are located along a hyperbola (see Fig. 1). For the layered soil considered in this paper, where the variations of permittivity between layers are relatively small, this remains true in first approximation [11]. The hyperbola is described by:

$$t = 2\sqrt{\frac{t_0^2}{4} + \frac{1}{v^2}(x - x_0)^2} \quad (1)$$

where $v = \frac{c}{\sqrt{\epsilon_{re}}}$ is the wave propagation speed in the soil, ϵ_{re} the effective relative dielectric permittivity, f is the GPR operation frequency, and c is the speed of the light in free space. Obviously, the antenna pattern limits the extend of this hyperbola. Note that, in this paper, we neglect the effect of the soil conductivity σ on v .

To detect the point scatterers, the following procedure is applied for each detected reflection: assuming that a reflection corresponds to a scatterer located at the vertical of the GPR (apex of the hyperbola) the theoretical hyperbola is computed for a number of effective dielectric permittivities (ϵ_{re}) and the number of points found along that hyperbola in the 'reflection binary image' (the number of detected reflections) is used as cost function. A 'detection binary image' is then created by keeping only the points where the cost function corresponding

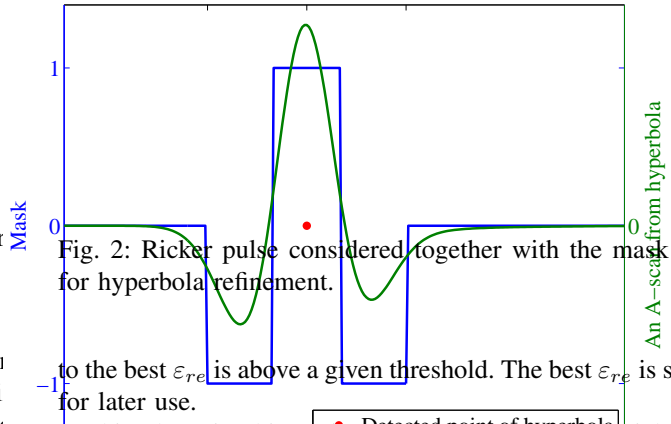


Fig. 2: Ricker pulse considered together with the mask used for hyperbola refinement.

to the best ϵ_{re} is above a given threshold. The best ϵ_{re} is stored for later use.

This 'detection binary image' is then segmented yielding a number of connected regions. For each region, only the point yielding the maximal cost function is kept as scatterer candidate. The (x_0, t_0) location together with the corresponding stored effective dielectric permittivity are then used as initial value for a second optimization of the hyperbola parameters.

C. Hyperbola refinement

This refinement step is performed on the original B-scan and takes into account the expected shape of point-scatterer reflections in the A-scans.

In first approximation, the reflected signal is simply a time-delayed version of the transmitted pulse. In this paper, we consider a ricker pulse as illustrated in Fig. 2. The shape of the transmitted signal is highly dependent of the GPR height above the ground and of the soil properties. Therefore, to increase robustness, the exact shape of the TX pulse is not used. Instead, only the knowledge that the reflection should exhibit a positive part surrounded by negative parts (or vice versa) is used to define a cost function for the refinement step. More precisely, the cost function computes the number of points with the appropriate sign in a rectangular mask around the theoretically hyperbola described by (1). This cost function is then optimized by varying the (x_0, t_0) location and soil effective dielectric permittivity ϵ_{re} , using as initial value the hyperbola parameters estimated in the previous step. This yields the parameters $(x_0, t_0, \epsilon_{re})$ of the best-fit hyperbola. Note that for a dispersive soil, the reflection will be a deformed version of the TX signal. Therefore, using only a crude model of the TX signal should also increase robustness in that case.

D. Estimation of soil dielectric permittivity and scatterer depth

As explained above, for a layered soil, the response of a point scatterer can still be approximated by an hyperbola but

obviously the corresponding effective dielectric permittivity is not equal to the scatterer layer permittivity. Instead, the dielectric permittivity of the layers above the scatterer layer and their thickness affect the estimated effective permittivity. Therefore, in the last processing step, the scatterer layer permittivity and the scatterer depth are derived from the estimated hyperbola parameters and the properties of the soil layers above the point-scatterer. Considering a monostatic radar and point-scatterer located in layer L , one can show that [11]:

$$ct_{0_L} = \sum_{i=1}^{L-1} d_i \sqrt{\epsilon_{r_i}} + \Delta z \sqrt{\epsilon_{r_L}} \quad (2)$$

$$\epsilon_{re} = \frac{ct_{0_L}}{\sum_{i=1}^{L-1} \frac{d_i}{\sqrt{\epsilon_{r_i}}} + \frac{\Delta z}{\sqrt{\epsilon_{r_L}}}} \quad (3)$$

with d_i and ϵ_{r_i} , the thickness and relative dielectric permittivity of layer i and Δz the depth of the scatterer in layer L (the distance to interface between layers L and $L - 1$).

Assuming that the soil properties are known up to layer $L - 1$, the above equations can be used to estimate layer L dielectric permittivity and the depth of the scatterer in that layer (Δz). Once layer L permittivity is known, its thickness d_i can be estimated from the time delay between the responses of its upper and lower interface that were detected as explained above in the reflection detection step.

If at least one point scatterer is detected in each layer, (2) and (3) can be used recursively, to estimate all soil layers permittivities and thicknesses, starting from the upper air layer ($i = 0$). As a byproduct, the depth of each detected scatterer is also found.

III. RESULTS

A. Finite-difference time-domain simulations

To evaluate the method presented in this paper, GPR B-scans were simulated in the time domain, using finite-difference time-domain (FDTD), with the GprMax2D software V 2.0 [12]. The monostatic GPR antenna is modeled as a hertzian horizontal dipole and is excited by a ricker pulse with a center frequency of 400 MHz and the responses are recorded within a time window of 50 ns.

The soil volume simulated has a width of 10 m and a depth of 3 m. The antenna is located 4 cm above the ground and scanned horizontally with a step of 5 cm for x ranging between 0.5 m and 9.5 m. The simulation cell size is 1 cm by 1 cm.

The soil layering and scatterer locations considered are illustrated in Fig. 3. Six scatterers were modeled as cylinders with a radius of 5 cm and a dielectric relative permittivity of 2.5. Three non-conductive soil layers were considered with dielectric permittivities of 5, 7, and 10.

B. Reflection detection

The detected reflections are shown in Figure 4. The hyperbolas corresponding to the six objects are clearly visible in the reflection binary image. The horizontal reflections corresponding to the three soil subsurfaces (including the ground surface) are also visible. The last horizontal reflection located

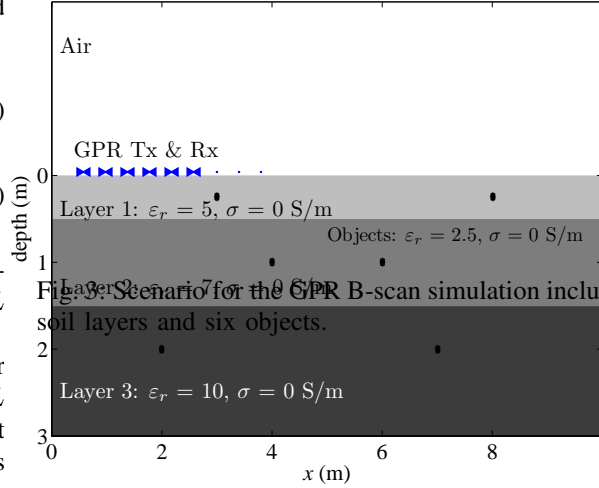


Fig. 3. Scenario for the GPR B-scan simulation including three soil layers and six objects.

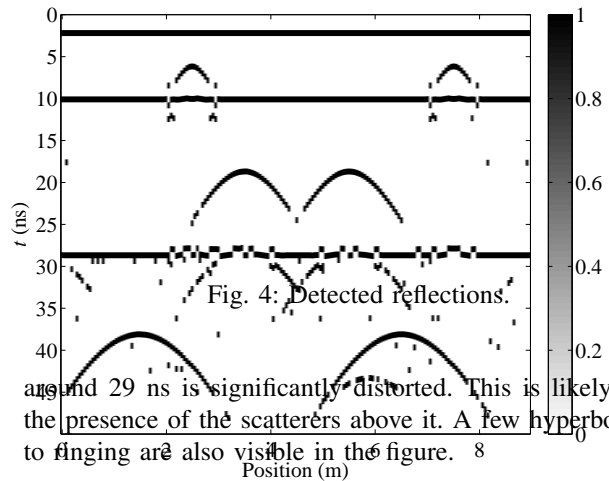


Fig. 4: Detected reflections.

and 29 ns is significantly distorted. This is likely due to the presence of the scatterers above it. A few hyperbolas due to fingering are also visible in the figure.

C. Hyperbola detection and refinement

For each reflection detected in Fig. 4, the fit of a hyperbola was attempted for ϵ_{re} ranging from 1 to 15 with a step of 0.5. Only the best fits were retained if the corresponding cost function was above a given threshold. The result is shown in Fig. 5 that also shows the regions obtained after segmentation and the corresponding best fit.

The hyperbola parameters are then refined considering ϵ_{re} ranging from -0.5 to +0.5 around the binary image best fit with a step of 0.01, x_0 ranging between -1 and +1 pixel around the binary image best fit and t_0 ranging from -0.5 to +0.5 times the length of the transmitted pulse. The corresponding hyperbolas are shown in Fig. 6 with the estimated values for ϵ_{re} shown above each hyperbola.

TABLE I: Result summary for a 3-layer soil

Layer#	d (m)	ε_r	Δz (m)	$\hat{\varepsilon}_{r_e}$	$\hat{\varepsilon}_r$	$\hat{d}(m)$	$\hat{\Delta z}$ (m)
1	0.5	5	0.25	4.42	5.75	0.51	0.247
2	1	7	0.5	5.43	5.95	1.11	0.504
3	∞	10	0.5	6.45	11.10	-	0.422

IV. CONCLUSIONS

An integrated approach allowing to detect point-scatterer and to recover the structure of a layered soil from a GPR B-scan is presented. The method includes the following steps: (1) reflection detection, (2) hyperbola detection, (3) refinement of hyperbola parameters and estimation of the corresponding scatterer location and soil effective dielectric permittivity, and (4) computation of scatterer depth and layer permittivity taking into account the properties of the upper layers.

The approach was evaluated using the FDTD simulations and showed good accuracy and high efficiency. For the scenario considered, all targets were detected and their depth was accurately recovered. Further the soil structure, including the number of layers as well as the permittivity and thickness of each layer, was accurately recovered.

V. ACKNOWLEDGMENT

This research was supported by Walloon region of Belgium in the framework of the SENSPORT projet (convention 1217720) of the WBGreen program. Also, this work benefited from the networking activities carried out within the EU funded COST Action TU1208 ‘‘Civil Engineering Applications of Ground Penetrating Radar’’.

REFERENCES

- [1] J. A. Huisman, S. S. Hubbard, J. D. Redman, and A. P. Annan, ‘‘Measuring soil water content with ground penetrating radar: A review,’’ *Vadose Zone Journal*, vol. 2, pp. 476–491, 2003.
- [2] L. W. Galagedara, G. W. Parkin, and J. D. Redman, ‘‘An analysis of the GPR direct ground wave method for soil water content measurement,’’ *Hydrological Processes*, vol. 17, pp. 3615–3628, 2003.
- [3] S. Lambot, E. C. Slob, I. van den Bosch, B. Stockbroeckx, and M. Vanclooster, ‘‘Modeling of ground-penetrating radar for accurate characterization of subsurface electric properties,’’ *IEEE Transactions on Geoscience and Remote Sensing*, vol. 42, pp. 2555–2568, 2004.
- [4] J. van der Kruk, ‘‘Properties of surface waveguides derived from inversion of fundamental and higher mode dispersive gpr data,’’ *IEEE T. Geoscience and Remote Sensing*, vol. 44, no. 10-2, pp. 2908–2915, 2006.
- [5] C. Strobbia and G. Cassiani, ‘‘Multilayer ground-penetrating radar guided waves in shallow soil layers for estimating soil water content,’’ *Geophysics*, vol. 72, no. 4, p. J17, 2007.
- [6] M. R. Mahmoudzadeh and S. Lambot, ‘‘Full-wave calibration of time- and frequency-domain ground-penetrating radar in far-field conditions,’’ *IEEE Trans. Geoscience and Remote Sensing*, 2013.
- [7] A. P. Annan, ‘‘GPR - history, trends, and future developments,’’ *Subsurface Sensing Technologies and Applications*, vol. 3, no. 4, pp. 253–270, 2002.
- [8] J. Wang and Y. Su, ‘‘Fast detection of GPR objects with cross correlation and hough transform,’’ *Progress In Electromagnetics Research C*, vol. 38, pp. 229–239, 2013.
- [9] N. Allroggen, J. Tronicke, M. Delock, and U. Boniger, ‘‘Topographic migration of gpr data with variable velocities,’’ in *Advanced Ground Penetrating Radar (IWAGPR), 2013 7th International Workshop on*, July 2013, pp. 1–5.
- [10] M. R. Mahmoudzadeh, ‘‘Automatic and fast detection of buried utilities positions and estimation of soil permittivity using GPR,’’ in *Proceedings of the Eleventh International Conference on Ground Penetrating Radar*, Columbus, Ohio, USA, 2006.

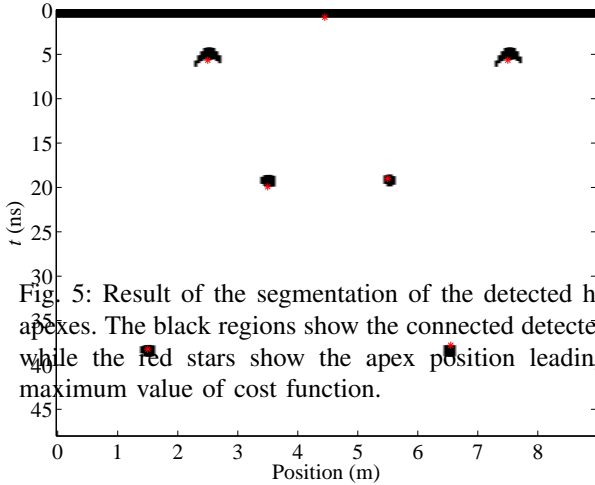


Fig. 5: Result of the segmentation of the detected hyperbola apexes. The black regions show the connected detected apexes while the red stars show the apex position leading to the maximum value of cost function.

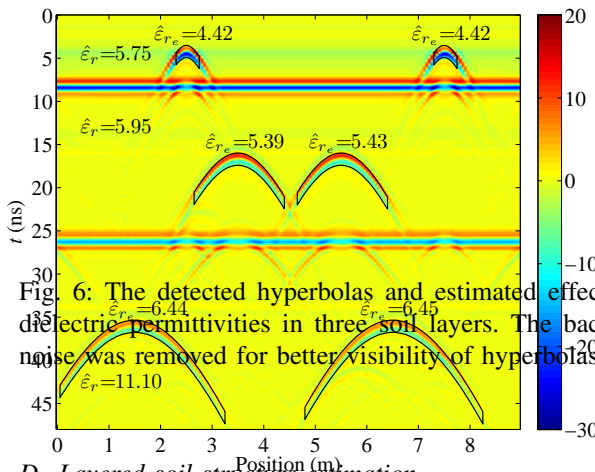


Fig. 6: The detected hyperbolas and estimated effective soil dielectric permittivities in three soil layers. The background noise was removed for better visibility of hyperbolas.

D. Layered soil structure estimation

The number of soil layers as well as the permittivity and thickness of each layer is automatically computed. The results are summarized in Table I which shows that layered soil structure is accurately recovered. The estimated layer permittivities are also shown above each hyperbola in Fig. 6.

The results clearly show that a significant error is made on the soil permittivity and scatterer depth estimation if the properties of the upper layers are not taken into account to convert the effective permittivities into layer permittivities.

- [11] W. Schneider, "The common depth point stack," *Proceedings of the IEEE*, vol. 72, no. 10, pp. 1238–1254, Oct 1984.
- [12] A. Giannopoulos, "Modelling ground penetrating radar by GPRMax," *Construction and Building Materials*, vol. 19, no. 10, pp. 755–762, 2005.